Materials Chemistry and Physics 132 (2012) 375–386

Contents lists available at SciVerse ScienceDirect

Materials Chemistry and Physics

journal homepage: www.elsevier.com/locate/matchemphys

Influence of divalent metal on the decomposition products of hydrotalcite-like ternary systems M^{II}–Al–Cr (M^{II} = Zn, Cd)

M.R. Pérez [a], I. Crespo [a], M.A. Ulibarri [a], C. Barriga [a], V. Rives [b], J.M. Fernández [a,*]

[a] Departamento de Química Inorgánica e Ingeniería Química, Campus de Rabanales, Universidad de Córdoba, Córdoba, Spain
[b] GIR-QUESCAT, Departamento de Química Inorgánica, Universidad de Salamanca, Salamanca, Spain

ARTICLE INFO

Article history:
Received 7 April 2011
Received in revised form 11 October 2011
Accepted 17 November 2011

Keywords:
Hydrotalcite
Double oxides
Spinels
Heat treatment

ABSTRACT

Layered double hydroxides (LDHs) containing M^{II}, Al^{III}, and Cr^{III} in the brucite-like layers (M = Cd, Zn) with different starting Al/Cr molar ratios and nitrate/carbonate as the interlayer anion have been prepared following the coprecipitation method at a constant pH: Zn^{II}–Al^{III}–Cr^{III}–CO_3^{2-} at pH = 10, and Cd^{II}–Al^{III}–Cr^{III}–NO_3^- at pH = 8. Two additional M^{II},Al^{III}–LDH samples (M = Cd, Zn) with chromate ions (CrO_4^{2-}) in the interlayer have been prepared by ionic exchange at pH = 9 and 8, respectively, starting from M^{II}–Al^{III}–NO_3^-. The samples have been characterised by absorption atomic spectrometry, powder X-ray diffraction (PXRD), FT-IR spectroscopy and transmission electron microscopy (TEM). Their thermal stability has been assessed by DTA-TG and mass spectrometric analysis of the evolved gases. The PXRD patterns of the solids calcined at 800 °C show diffraction lines corresponding to ZnO and $ZnAl_{2-x}Cr_xO_4$ for the Zn-containing samples, and diffraction lines attributed to CdO and $CdCr_2O_4$ and $(Al,Cr)_2O_3$ for the Cd-containing ones. Additionally a minority oxide, Cd_2CrO_5, is observed to Cd^{II}–Al^{III}–LDH samples with chromate ions in the interlayer.

1. Introduction

Layered double hydroxides (LDH), a wide group of compounds also known as hydrotalcite-like compounds, are inexpensive and easy to synthesize. In spite of some similarities with clay minerals, and the existence of some of them in Nature, they constitute another class of layered materials, as it has been stated by Bergaya and Lagaly [1], owing to the synthetic origin of most of them. The partial isomorphic substitution of M^{II} cations in octahedral coordination by M^{III} cations in the brucite layer, $M(OH)_2$, gives rise to positive charges in the layers which are electrically balanced by anions in the interlayer space. The general formula $[M^{II}_{1-x}M^{III}_x(OH)_2]^{x+}A^{m-}_{x/m}\cdot nH_2O$ is used to represent these compounds, where the identities of the divalent and trivalent cations (M^{II} and M^{III}, respectively), the interlayer anion (A^{n-}) and the stoichiometric coefficient (x) may be assorted over a wide range. Control of the precipitation conditions enables to prepare a large number of layered double hydroxides with different interlayer anions and metal cations in the brucite layers. The metal cations are homogeneously distributed in the layers when the coprecipitation method is used [2]. In this sense, it is possible to prepare tailored LDHs. The incorporation of different metals in the layer and/or interlayer makes these compounds suitable as catalysts or catalyst precursors. LDH with M^{II} = Zn, M^{III} = Al and A^{m-} = CO_3^{2-}, NO_3^- can be used to incorporate one or more transition metal cations in the layer, when Zn^{2+} and/or Al^{3+} cations are totally or partially replaced. The transition metal induces a certain degree of acidity [3] so it is possible to tune the basic strength of a series of ternary LDHs according to their pursued application or use [4].

Broadly speaking, the thermal decomposition of LDHs is well known; calcination at intermediate temperatures (450–600 °C) yields an amorphous phase $M^{II}_{1-x}M^{III}_xO_{1+x/2}$ which is turned into crystalline phases, the divalent oxide MO and a mixed oxide (usually $M^{II}M^{III}_2O_4$ spinel), at higher temperatures; the LDHs are potential precursors to such spinels. Meng et al. [5] have reported that when the divalent cation is Zn the zincite phase obtained can be eliminated by dissolution in aqueous NaOH resulting in the formation of the pure spinel phase. Furthermore, the products obtained from LDHs show several advantages if compared to those prepared by the ceramic process: an increase in surface area and pore volume, formation of a homogenous spinel phase, the ferrite spinel enhances their saturation magnetization [6], etc.

On the other hand, the final calcination products from ternary systems depend on the nature of the cations and their location (layer or interlayer space) [7,8,10]. Consequently different mixed oxides could be obtained to be used as catalysts or catalyst precursors, ZnO and CdO and mixtures as photocatalyst [11–13]. Although few data have been reported regarding ternary systems in comparison with binary ones [14–16] the research in this area has increased in the last ten years due to their interest in catalysis [17,18].

* Corresponding author. Tel.: +34 957 218648; fax: +34 957 218621.
E-mail address: um1feroj@uco.es (J.M. Fernández).

0254-0584/$ – see front matter © 2011 Elsevier B.V. All rights reserved.
doi:10.1016/j.matchemphys.2011.11.040

In the present paper we report on the synthesis of layered double hydroxides (LDHs) containing M^{2+}, Al^{3+}, and Cr^{3+} in the brucite-like layers (M = Cd, Zn) with different starting Al/Cr molar ratios and with nitrate/carbonate as interlayer anions. They have been prepared following the coprecipitation method at constant pH. Two additional M^{II},Al^{III}–LDH samples (M = Cd, Zn) interlayered with chromate ions (CrO_4^{2-}) have been prepared by ionic exchange at pH = 9 and 8, respectively. The mixed oxides obtained after calcination of M^{II},Al hydrotalcites with different amounts of Cr (either in the layers or in the interlayer) have been characterised, and the effect of the initial location of this metal (in the layer or in the interlayer) on the nature and/or crystallinity of the phases formed has been also studied. It will be of interest knowing how the change of divalent metal (Cd or Zn) modifies the precise nature of the calcination products.

2. Experimental

2.1. Preparation of the samples

Briefly, samples containing Zn^{2+}, Al^{3+}, and Cr^{3+} in the layers were prepared by dropwise addition of aqueous solutions (200 mL) of the corresponding nitrates ($Zn(NO_3)_2{\cdot}6H_2O$ and $Al(NO_3)_3{\cdot}9H_2O$ from Panreac 99% and $Cd(NO_3)_2{\cdot}4H_2O$ from Sigma–Aldrich 99%) with different starting molar ratios [Zn/(Al + Cr) = 2 in all cases and Al/Cr = 0, 1, 4, ∞] into a reaction flask containing 200 mL of 0.3 M Na_2CO_3 and of 1.5 M NaOH aqueous solution with constant stirring for 30 min; pH was kept constant at 10, with a 691 pH-meter coupled to an automatic 725 Dosimat dispenser, from Metrohm, and the suspension was stirred at room temperature for 1 h. The products were further stirred for 24 h, centrifuged, washed with distilled water and dried at 60 °C for 24 h. Samples containing Cd^{2+}, Al^{3+}, and Cr^{3+} in the layers were prepared following a similar procedure, but using boiled water and bubbling N_2 during the reaction to avoid carbonation of the samples. These are named as *M*AlCr-*I*-*X*, where *M* stands for Zn or Cd, *I* for nitrate (N) or carbonate (C) and *X* for the nominal Al/Cr molar ratio. Solids were calcined at selected temperatures for 3 h in air and named *M*AlCr-*I*-*X*-*T*, where *T* stands for the calcination temperature (150, 250, 300, 400, 500, 600 and 800 °C).

To prepare additional samples containing chromate ions in the interlayer, a M^{II},Al^{III}-nitrate hydrotalcite precursor (M = Cd, Zn) was synthesized by dropwise addition of an aqueous solution (200 mL) of the M(II) (0.2 M) and Al (0.1 M) nitrates in distilled and boiled water into a three-neck reaction flask containing 200 mL of 1 M $NaNO_3$ (in deionised water) with constant stirring for 1 h; pH was kept constant at 8, using a 0.5 M NaOH aqueous solution. It was kept on stirring at room temperature for 1 h. During reaction, nitrogen was bubbled through the suspension to avoid carbonation of the samples from atmospheric CO_2. The solids thus obtained were filtered, washed, and suspended in decarbonated water, and a solution of chromate (3.00 g of K_2CrO_4 in 200 mL of water) was dropwise added for 1 h; pH was maintained at 8.0 for M = Zn and at pH = 9 for M = Cd. Stirring was continued at room temperature for 48 h. The precipitate was aged in the mother liquor for 24 h, filtered, washed, dried at 60 °C for 24 h, and then calcined at selected temperatures for 3 h in air. While the uncalcined samples will be named as MAl–CrO_4, the calcined ones will be named as MAl-*CrO_4*-*T*, where *T* stands for the calcination temperature, in °C.

2.2. Experimental techniques

Element chemical analyses for Zn, Cd, Al and Cr were carried out by atomic absorption spectrometry in an AA-3100 instrument from Perkin Elmer.

Powder X-ray diffraction (PXRD) patterns were recorded in a Siemens D-5000 instrument, using CuKα radiation (λ = 1.5418 Å). Diffraction lines due to the Al sample holder were recorded in some diagrams and were used as a sort of internal reference to determine more precisely the positions of the diffraction peaks. Identification of the crystalline phases has been carried out by comparison with the JCPDS files [19].

Thermogravimetric (TG) and differential thermal analyses (DTA) were carried out in a Setsys Evolution 16/18 instrument from SETARAM, in air for Zn-containing hydrotalcites or flowing N_2 (from Carburos Metálicos, Spain) for Cd-containing hydrotalcites at a heating rate of 5 °C min^{-1}. Mass Spectrometry Analysis of the gases evolved during the thermal decomposition was carried out in a EM-Pfeiffer Vacuum Omnistar.

FT-IR spectra were recorded by the KBr pellet technique in a Perkin Elmer Spectrum One Fourier Transform instrument.

Microstructural characterisation of the materials was carried out using a JEOL 200CX TEM equipment.

3. Results and discussion

3.1. Hydrotalcite-type materials

All MAlCr-I-X samples showed PXRD patterns (Fig. 1) corresponding to well-crystallized hydrotalcites with rhombhohedral 3R symmetry [20], and d_{003} spacings consistent with the presence of carbonate (7.56–7.8 Å) or nitrate (8.0–8.7 Å) in the interlayer.

A least squares adjustment programme has been used [21] for calculating lattice parameters *a* and *c*; the values are included in Table 1.

Brindley and Kikkawa [22] and Brown [23] have shown that the *c* parameter depends on the thickness of octahedral sheets, the anions size and their orientation within the interlayer space, and the electrostatic attraction between different layers, and the *a* parameter depends mainly on the cations size. In our case, an increase in the *c* parameter has been found when the amount of Cr is steadily increased (i.e., the Al^{3+}/Cr^{3+} ratio is decreased).

The values of parameter *a* show a slight increase with the progressive increase in chromium content, probably due to the larger size of the Cr^{3+} than Al^{3+} (0.775 and 0.675 Å, respectively) [24,25]. This behavior is similar to that observed for the Cd–Fe–Al system [8], previously reported.

Similarly to the results obtained by Brindley and Kikkawa [22], the variation of the *a* parameter can be correlated with the Al/Cr ratio. On a first approach, we can take that in an ideal octahedral sheet $a = \sqrt{2}\cdot(M{-}O)$, where M–O is the metal–oxygen distance. The average radius of the cation can be calculated from the chemical composition, according to:

$$\bar{r} = 0.66 \cdot r_{Zn} + (0.33 - x) \cdot r_{Al} + x \cdot r_{Cr} = 0.66 \cdot r_{Zn} + 0.33 \cdot r_{Al} + x \cdot (r_{Cr} - r_{Al})$$

On plotting the values of parameter *a* vs. the Cr content for samples ZnAlCr-C-X and CdAlCr-N-X straight lines are obtained, which slopes, $\sqrt{2}\cdot(r_{Cr} - r_{Al})$, were 0.14 and 0.09, respectively. These values acceptably agree with the theoretical value 0.113, which confirms the presence of the three cations in the layer structure of the hydrotalcite.

The FWHM values measured for the (0 0 3) diffraction line and the calculated crystalline size (Table 1) indicate that a substantial reduction in the crystallinity of the samples takes place when the presence of chromium increases into the layer, due to the distortion produced in the layer by the larger size of chromium (0.775 Å) in relation to aluminum (0.675 Å) [9].

The PXRD patterns of samples MAl–CrO_4 are also shown in Fig. 1. Comparing to those of the series *M*AlCr-*I*-∞ a lower crystallinity

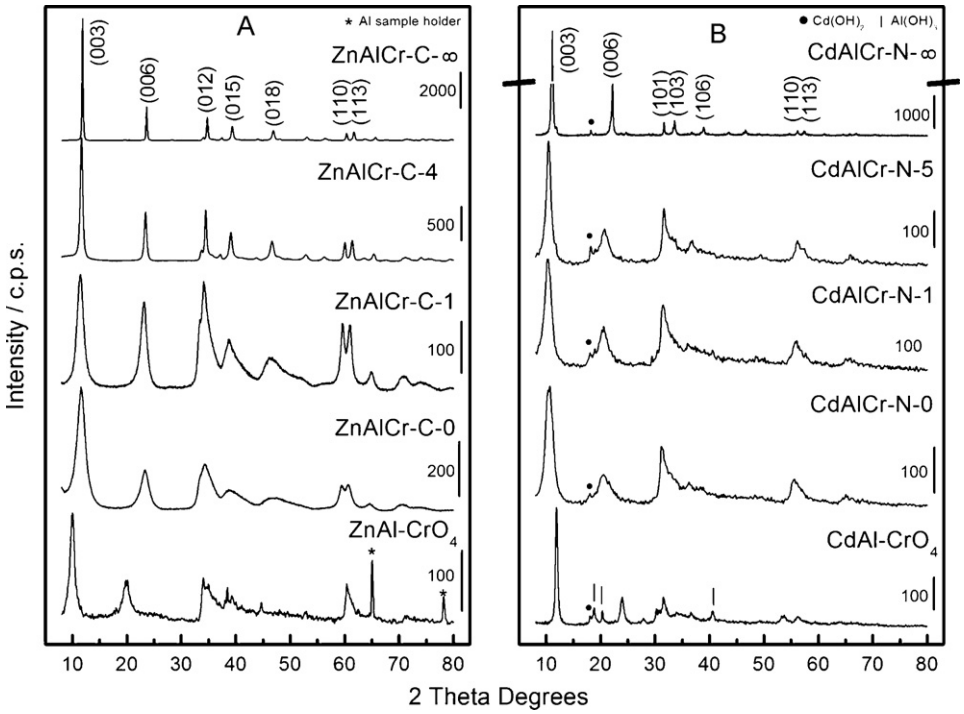

Fig. 1. PXRD diagrams of samples ZnAlCr-C and ZnAl–CrO_4 (A) and samples CdAlCr-N and CdAl–CrO_4 (B).

is observed, because the anion exchange causes a broadening of the peaks [26]. Lattice parameters *c* and *a* for these two samples are also included in Table 1. The PXRD spacing for planes (0 0 3) of sample ZnAl–CrO_4 was 8.86 Å (assuming a rhombohedral 3R symmetry [27,28]), and from the thickness of the brucite-like layer (4.8 Å) [29], a value of 4.06 Å, similar to that reported by Miyata and Okada [30], can be calculated for the interlayer space. On the other hand, the diagram for sample CdAl–CrO_4 corresponds to a well-crystallized hydrotalcite, but the presence of small impurities of $Cd(OH)_2$ (40-0760) (JCPDS 1995) and $Al(OH)_3$ (3-1377) [19] is also concluded. The value d_{003} = 7.43 Å is very small to accommodate the anion CrO_4^{2-} whose size is 4.8 Å [31]; taking into account the sheet thickness (4.8 Å) gets a value of 9.6 Å, suggesting *grafting* of the chromate anion to the brucite layers [32,33]. A similar behavior is observed for ZnAl–CrO_4 when it is dried at higher temperature, 150 °C, decreasing d_{003} value until 7.2 Å (PhD I. Crespo, not shown).

The values of parameter *a* and the FWHM values for the (0 0 3) reflexion for all samples of the *M*AlCr-*I*-∞ series are close to each other, although they are larger than those corresponding to the *M*AlCr-*I*-∞ hydrotalcite, and much lower than that measured for samples with Cr^{3+} cations in layer, which indicates a minimal structural alteration of the layer as a result of the exchange process.

Microphotographs show in all cases hexagonal particles as for other hydrotalcite-type systems [34]. Transmission electron micrographs for selected samples ZnAlCr-C-∞, ZnAlCr-C-1 and ZnAlCr-C-0 are shown in Fig. 2. The size of the particles is similar in all samples. However, the presence of large pores in the chromium-rich samples may be noticed. Electron micrographs for sample ZnAl–CrO_4 shows that the particles have a rounded shape, but above all stresses the large size of the particles.

The FT-IR spectra of the samples prepared (Fig. 3) show the typical bands of the hydrotalcite-like compounds [7,31,35–39] with a very intense and broad absorption band around 3500 cm^{-1} which is due to the stretching mode of layer hydroxyl groups as well as to the stretching mode of interlayer water molecules. Hydrogen bonding between the water molecules and the interlayer anions also accounts for broadening of this band in the low wavenumbers side. The bending mode of water molecules gives rise to a rather weak band around 1620 cm^{-1}, and the bands associated to lattice vibrations of the brucite-like layers appear below 800 cm^{-1}. In addition, bands corresponding to the different interlayer anions are recorded

Table 1
Lattice parameters *c* and *a* (Å), FWHM (°2θ) and crystalline size corresponding to reflexion (0 0 3) for samples MAlCr-I-X and $MAlCrO_4$ (standard deviation in parenthesis).

Sample	ZnAlCr-C-∞	ZnAlCr-C-4	ZnAlCr-C-1	ZnAlCr-C-0	$ZnAlCrO_4$
c	22.67(3)	22.72(4)	22.81(3)	23.39(4)	26.58(3)
a	3.069(2)	3.080(3)	3.087(1)	3.118(4)	3.07(1)
FWHM	0.220(1)	0.520(3)	1.376(3)	1.602(2)	0.680(3)
Crystalline size[a] (Å)	379.5(2)	168.5(2)	60.97(3)	52.21(2)	122.51(4)
Sample	CdAlCr-N-∞	CdAlCr-N-5	CdAlCr-N-1	CdAlCr-N-0	$CdAlCrO_4$
c	23.94(4)	25.43(2)	26.09(3)	25.38(1)	22.30(4)
a	3.272(2)	3.276(4)	3.287(4)	3.302(2)	3.268(4)
FWHM	0.214(1)	0.956(1)	1.410(1)	1.617(1)	0.442(2)
Crystalline size[a] (Å)	389.67(3)	87.22(2)	59.14(2)	51.57(1)	189.04(3)

[a] Crystalline size calculated using Scherrer formula.

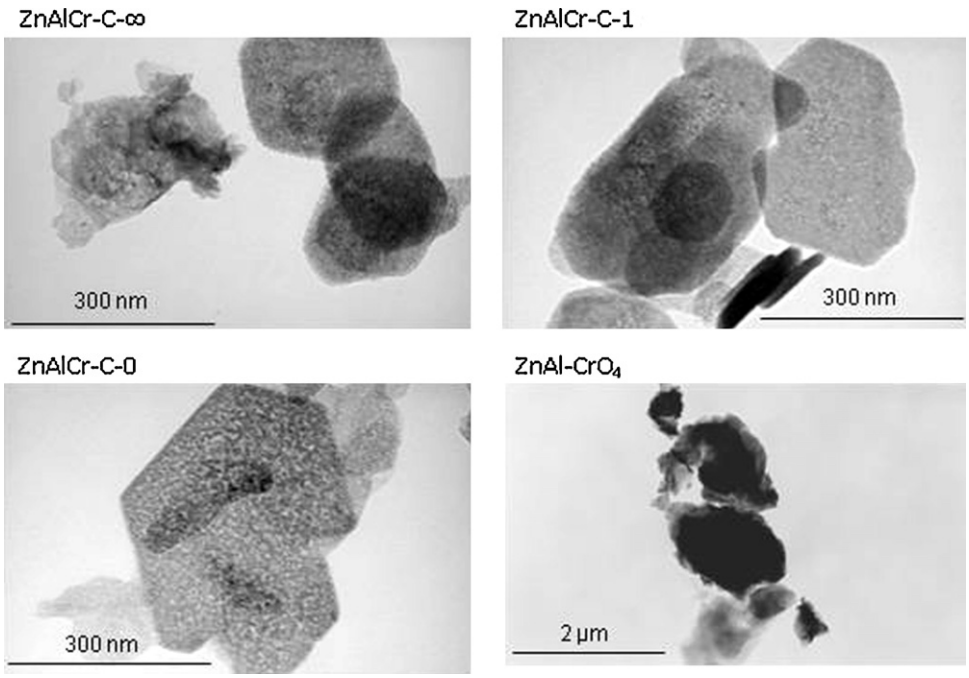

Fig. 2. TEM micrographs of samples ZnAlCr-C-0, ZnAlCr-C-1, ZnAlCr-C-∞ and ZnAl–CrO_4.

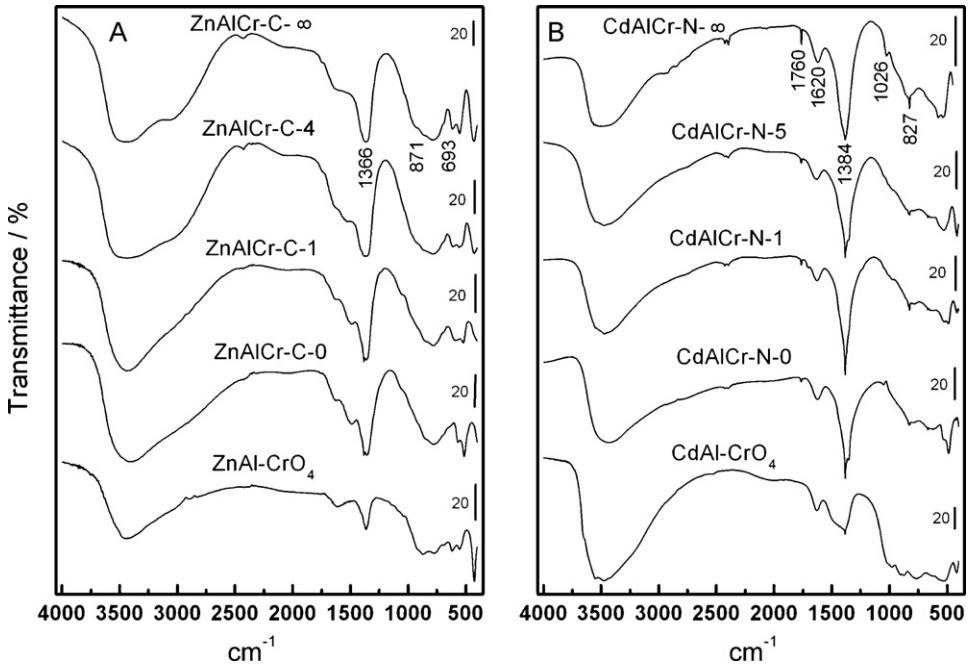

Fig. 3. FT-IR spectra of samples ZnAlCr-C and ZnAl–CrO_4 (A) and samples CdAlCr-N and CdAl–CrO_4 (B).

Table 2
Assignment of the bands (cm^{-1}) recorded in the FT-IR spectra of samples ZnAlCr-C-X, ZnAl–CrO_4 and of free CrO_4^{2-}.

	ZnAlCr-C-∞	ZnAlCr-C-4	ZnAlCr-C-1	ZnAlCr-C-0	ZnAl–CrO_4	Free CrO_4^{2-} [37]
ν_{O-H}	3437	3450	3423	3410	3438	
δ_{H-O-H}	1642	1638	1617	1617	1609	
$\nu_3(CO_3^{2-})$	1544, 1366	1528, 1367	1484, 1360	1484, 1355	1362	
$\nu_1(CO_3^{2-})$	–	1055	1057	1058	–	
$\nu_2(CO_3^{2-})$	871	871	843	841	–	
$\nu_4(CO_3^{2-})$	693	693	692	691	690	
ν_{Cr-O}	–	–	–	–	869	890
δ_{Cr-O}	–	–	–	–	–	378
ν_{M-O}	951, 783, 615 552, 428	938, 780, 608 553, 428	917, 780, 591 520, 402, 387	915, 780 568, 513, 382	927, 772, 618 555, 425	

Table 3
Assignment of the bands (cm^{-1}) recorded in the FT-IR spectra of samples CdAlCr-N-X, CdAl–CrO_4 and of free CrO_4^{2-}.

	CdAlCr-N-∞	CdAlCr-N-5	CdAlCr-N-1	CdAlCr-N-0	CdAl–CrO_4	Free CrO_4^{2-} [37]
ν_{O-H}	3491	3477	3474	3429	3550, 3476	
δ_{H-O-H}	1618	1630	1629	1623	1634	
$\nu_3(NO_3^-)$	1384	1383	1384	1384	1384	
$\nu_1(NO_3^-)$	1026	–	–	1049	–	
$\nu_2(NO_3^-)$	826	827	826	825	–	
$\nu_4(NO_3^-)$	–	669	668	669	–	
$\nu_1 + \nu_4$	1762	1763	1765	1765	–	
ν_{Cr-O}	–	–	–	–	876	890
δ_{Cr-O}	–	–	–	–	–	378
ν_{M-O}	578, 539, 426	530, 414	531, 489, 419	534, 487	979, 767, 531, 420	

Table 4
Element chemical analysis data (metals) for samples ZnAlCr-C-X, ZnAl–CrO_4, CdAlCr-N-X, CdAl–CrO_4.[d]

Sample	Zn[a]	Cd[a]	Cr[a]	Al[a]	Zn^{2+}/M^{3+}[b,c]	Cd^{2+}/M^{3+}[b,c]	Al/Cr[b]
ZnAlCr-C-∞	38.3	–	0.0	8.2	1.9	–	∞
ZnAlCr-C-4	36.9	–	3.4	6.2	1.9	–	3.5
ZnAlCr-C-1	37.4	–	7.9	4.0	1.9	–	1.0
ZnAlCr-C-0	36.8	–	15.7	0.0	1.8	–	0.0
ZnAl–CrO_4	35.5	–	6.0	7.8	1.9	–	2.5
CdAlCr-N-∞	–	47.4	0.0	6.0	–	1.9	∞
CdAlCr-N-5	–	44.3	2.0	5.2	–	1.7	0.2
CdAlCr-N-1	–	43.3	5.2	2.7	–	1.9	1.0
CdAlCr-N-0	–	48.3	10.9	0.0	–	2.1	0.0
CdAl–CrO_4	–	34.4	3.7	12.7	–	0.7	6.6

[a] Mass percentage.
[b] Molar ratio.
[c] Cations in the layers.
[d] Values have been rounded to one figure after the decimal point.

between 1760 and 668 cm^{-1}. The detailed assignment of the bands is summarised in Tables 2 and 3.

Concerning the lattice vibrations (Tables 2 and 3) all samples show five bands [40] that can be related to the D_{3d} symmetry of distorted octahedra and ordering of the cations in the layer. The presence of three different cations in the layers lead to rather broad, ill-defined, bands if compared to similar samples with only two cations, (Al/Cr = ∞ or 0); this could be explained by a lower cation ordering in the layer. Furthermore, replacement of Al by Cr leads shifts the positions of the bands to lower wavenumbers. This is due to the larger atomic mass of Cr with respect to Al [41].

The bands originated by interlayer carbonate anions (Table 2) are recorded at wavenumbers somewhat lower than those assigned to "free" carbonate anions, as it has been reported and explained in previous studies [42–44].

The bands corresponding to nitrate vibrations (Table 3) are also recorded at wavenumbers somewhat lower than those corresponding to "free" nitrate anions; that due to mode ν_3 is recorded around 1384 cm^{-1}, while that close to 826 cm^{-1} is due to mode ν_2. Mode ν_4 (680 cm^{-1} for free nitrate) is recorded as a very weak and sharp band at around 669 cm^{-1} when chromium is added to the structure of the hydrotalcite. Mode ν_1 is forbidden in IR for a D_{3h} symmetry, but the characteristic combination mode [41] $\nu_1 + \nu_4$ is recorded as a weak, extremely sharp band around 1760 cm^{-1}.

Incorporation of chromate in the interlayer gives rise to a band at 869 cm^{-1} for ZnAl–CrO_4 and at 876 cm^{-1} for CdAl–CrO_4. Recording of the bands due to interlayer chromate species at lower wavenumbers than for the free anion (Tables 2 and 3) indicates a weakening of the Cr–O bond due to the interaction through hydrogen bonding with water molecules or hydroxyl groups of the layer. Nevertheless, a small contamination by carbonate and nitrate cannot be ignored, due to the high pH of the solution during synthesis of the samples.

Absorption atomic spectroscopy data (metals) for samples ZnAlCr-C-X, ZnAl–CrO_4, CdAlCr-N-X, CdAl–CrO_4 have been included in Table 4. The values calculated for samples ZnAlCr-C-X are consistent with the concentration of the cations in the starting solutions, indicating that this type of hydrotalcites can be easily prepared with a variety of different metal molar ratios without significant deviations of the initial concentration of the salt metals. The molar Zn/Al ratio for sample ZnAl–CrO_4 is fairly consistent with that for sample ZnAlCr-N-∞ used as precursor of the former. The Al/Cr ratio is somewhat larger than the expected value of 2, probably because of the presence of a small amount of CO_3^{2-} as concluded from the FT-IR study. The values determined for samples CdAlCr-N-X are also consistent with the metal concentrations in the starting solutions. The Cd/Al ratio for sample CdAl–CrO_4 is much lower than the expected value, suggesting that a partial dissolution of Cd^{2+} occurred during the process of exchange, and the Al/Cr ratio, which should be equal to 2, amounts a value of 6.6, what indicates that the positive charge of the layers is not balanced exclusively by CrO_4^{2-} anions, but also by NO_3^- or CO_3^{2-}, which presence was concluded from the FT-IR spectra thus giving rise to the calculated formula included in Table 5.

Table 5
Formulae proposed for the samples.

Sample	Formula
ZnAlCr-C-∞	$[Zn_{0.66}Al_{0.34}(OH)_2](CO_3)_{0.17}\cdot 0.7H_2O$
ZnAlCr-C-4	$[Zn_{0.66}Al_{0.27}Cr_{0.07}(OH)_2](CO_3)_{0.17}\cdot 0.6H_2O$
ZnAlCr-C-1	$[Zn_{0.66}Al_{0.17}Cr_{0.17}(OH)_2](CO_3)_{0.17}\cdot 0.7H_2O$
ZnAlCr-C-0	$[Zn_{0.64}Cr_{0.36}(OH)_2](CO_3)_{0.18}\cdot 0.9H_2O$
CdAlCr-N-∞	$[Cd_{0.66}Al_{0.34}(OH)_2](NO_3)_{0.34}\cdot 0.4H_2O$
CdAlCr-N-5	$[Cd_{0.63}Al_{0.31}Cr_{0.06}(OH)_2](NO_3)_{0.37}\cdot 0.3H_2O$
CdAlCr-N-1	$[Cd_{0.66}Al_{0.17}Cr_{0.17}(OH)_2](NO_3)_{0.34}\cdot 0.2H_2O$
CdAlCr-N-0	$[Cd_{0.67}Cr_{0.33}(OH)_2](NO_3)_{0.33}\cdot 0.1H_2O$
ZnAl–CrO_4	$[Zn_{0.66}Al_{0.34}(OH)_2](CrO_4)_{0.14}(CO_3)_{0.03}\cdot 0.8H_2O$
CdAl–CrO_4	$[Cd_{0.39}Al_{0.61}(OH)_2]X_{0.61/n}{}^{n}\cdot 0.1H_2O$

X = CrO_4^{2-}, NO_3^-, CO_3^{2-}.

The above results on metal chemical analysis and the water content, as calculated from the TG analysis, permit to calculate the formulae of the samples prepared, Table 5. However, we want to stress that these are only approximate formulae, as a small amount

of $Cd(OH)_2$ exists in samples containing three metals in the layer, and $Cd(OH)_2$ and $Al(OH)_3$ in the sample with interlayer CrO_4^{2-} species.

Thermal decomposition of hydrotalcites usually takes place in three steps, namely, dehydration, dehydroxylation and decomposition of the interlayer anions, although in most of the cases steps two and three overlap [45]. In some cases *plateaux* are recorded in the TG diagram between two consecutive mass loss steps. However, for the samples here studied, no well-defined plateau was recorded, and so the total mass loss, instead of that corresponding to the first step, has been used to determine the water content of the samples, by applying simple stoichiometric relationships, once the nature of the solid residues after complete decomposition is known from PXRD analysis. Usually the number of interlayer water molecules can be related to the interlayer concentration of anions [43], i.e., as the water concentration increases that of the anion decreases. Consequently, samples with interlayer NO_3^- have lower water content interlayer than those with CO_3^{2-}, as two nitrate anions, but only one carbonate anion, are required to balance two positive charges in the layer anions.

The DTA-TG diagrams of the ZnAlCr-C-X samples are shown in Fig. 4A. The DTA diagram for sample ZnAlCr-C-∞ shows only one endothermic effect attributed to overlapping of various effects: lost of interlayer water, dehydroxylation (that occurs at temperatures lower than in other hydrotalcites because the low temperature decomposition of $Zn(OH)_2$, 175 °C [46]) and finally, decarbonation of samples. For samples ZnAlCr-C-4 (not shown) and ZnAlCr-C-1 two endothermic effects at 212 and 262 °C and at 195 and 263 °C, respectively, have been recorded and four effects for sample ZnAlCr-C-0 at 149, 211, 308 and 430 °C. It can see that the introduction of Cr^{3+} in the layer gives rise to a decrease in temperature at which water is lost. This may be linked with the decrease of hydrogen bridges between interlayer water molecules and carbonate anions [37]. In this last sample, ZnAlCr-C-0, collapsing of the structure occurs above 300 °C and an exothermic effect appears at 430 °C. This effect has been attributed to oxidation of Cr^{3+} to Cr^{6+} with the subsequent formation of chromate species [44,47]. The mass loss is very similar for all samples, corresponding to 34–35% of the initial sample mass, because of the charge of the layer is the same and then, the amount of interlayer anion is similar in all cases.

Concerning samples CdAlCr-N-X (Fig. 4B), is noticeable that the sample CdAlCr-N-0, Fig, 4B, shows a very well-defined peak at 265 °C, but this peak is split in samples containing aluminum. The effect between 350 and 500 °C corresponds to the loss of the nitrate anions from the interlayer, as confirmed from the analysis by mass spectrometry of the gases evolved (Fig. 5), where signals at $m/z = 30$ and $m/z = 46$ corresponding to NO and NO_2, respectively, are recorded. Finally, another endothermic effect has been observed, centered around 620–650 °C corresponding to a O_2 loss detected by mass spectrometry (Fig. 5) through of signal of relationship $m/z = 32$. This effect has been observed in systems where ion Cr^{3+} is present [44], and it is absent in others with similar structure with cations not susceptible to be oxidized [48,49]. It can be associated to the reduction of Cr^{6+} to Cr^{3+} to form a Cd^{2+}–Cr^{3+} mixed oxide. This means that a previous oxidation of Cr^{3+} to Cr^{6+} has taken place, but it was not detected in systems containing chromium and with CO_3^{2-} as the interlayer anion [11,44] when the analysis was recorded in an inert atmosphere. Oxidation of Cr^{3+} has been probably assisted by the interlayer anion, which in this case was NO_3^-, and which oxidizing ability is well known; it can oxidize Cr^{3+} to Cr^{6+} while itself being reduced to NO_2 and NO, which presence has been confirmed by mass spectroscopy. The total mass loss for samples CdAlCr-N-∞, CdAlCr-N-1 and CdAlCr-N-0 were between 26.0% and 28.0%.

The DTA diagrams for samples ZnAl–CrO_4 and CdAl–CrO_4 are also included in Fig. 4. Sample ZnAl–CrO_4 shows five endothermic effects. The first effect occurs at 127 °C and it is associated to the loss of interlayer water molecules, but it is recorded at lower temperatures than those for samples containing carbonate as the interlayer anion. This decrease in the temperature needed to release these

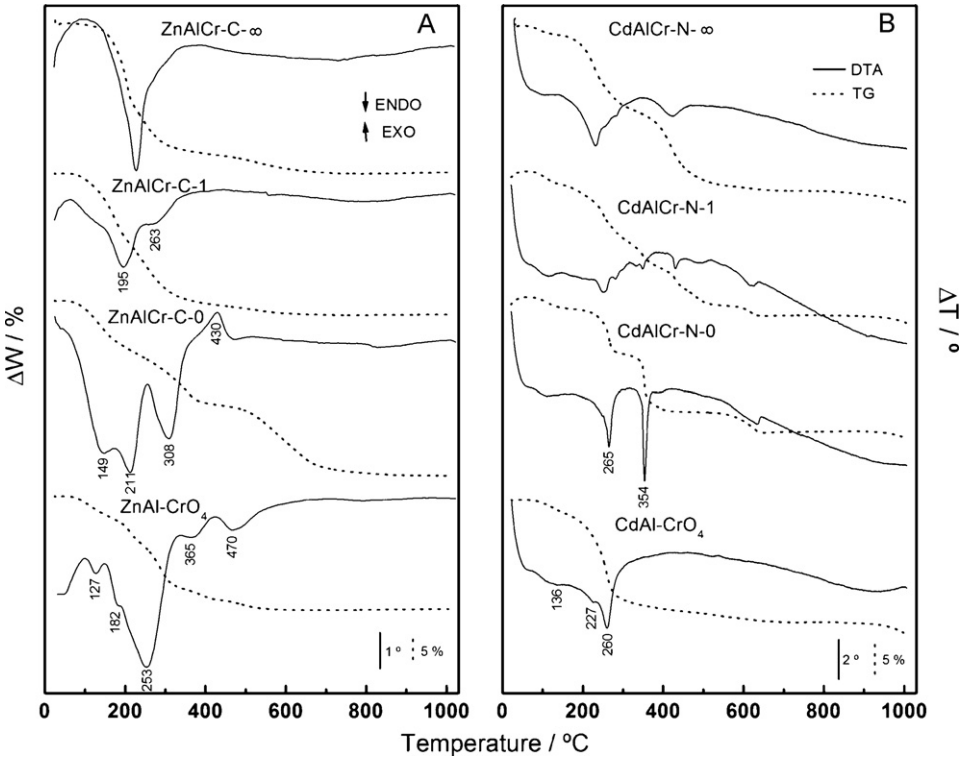

Fig. 4. TG (dotted lines) and DTA (solid lines) profiles of the samples ZnAlCr-C, CdAlCr-N, ZnAl–CrO_4 and CdAl–CrO_4.

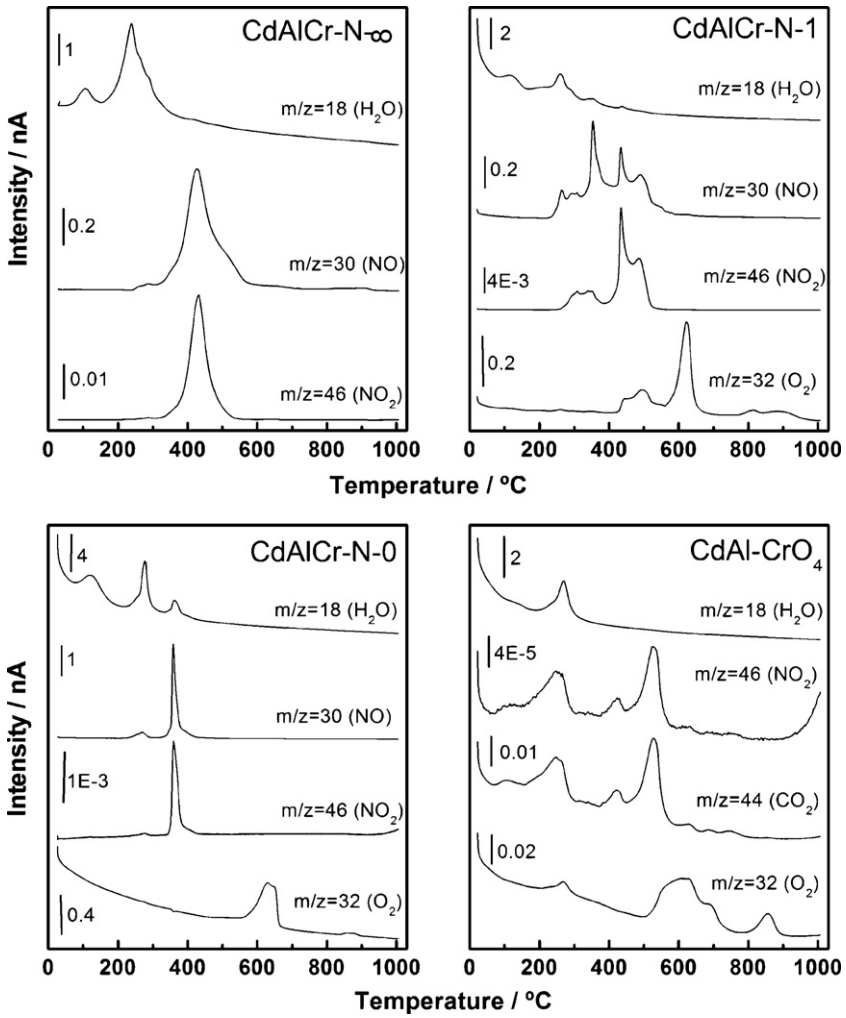

Fig. 5. Mass spectrometry diagrams of gases evolved during thermal decomposition of samples CdAlCr-N and CdAl–CrO_4.

water molecules can be originated by a smaller number of bridges hydrogen between water and the interlayer anion as noted in the infrared spectrum of this sample. The endothermic effects at 182 °C and 253 °C can be assigned to dehydroxylation and collapse of the structure. The endothermic effects at 365 °C and 470 °C may be due to the decomposition of the CrO_4^{2-} anion and the reduction to Cr^{3+} species to form a spinel phase, as it will be discussed below using PXRD data included in Fig. 6. The mass loss recorded was 26%.

The DTA diagram for sample CdAl–CrO_4 (Fig. 4) shows several endothermic effects from room temperature to 300 °C and it is similar to the curve recorded for samples ZnAl–CrO_4. The analysis of the gases evolved (Fig. 5) during the decomposition of this sample shows the release of four species: H_2O (m/z = 18) from interlayer water loss dehydroxylation of the layers, oxygen (m/z = 32) as a result of the reduction of Cr^{6+} to Cr^{3+}, and finally CO_2 (m/z = 44) and NO_2 (m/z = 46) produced through decomposition of carbonate and nitrate anions existing as impurities, as shown by the infrared spectra and discussed above. The total mass loss was 38.3%.

3.2. Calcination products

In order to insight in the knowledge of the crystalline phases existing in the samples after calcination the samples were calcined at temperatures before and after those of the main DTA effects. Samples ZnAlCr-C-X and ZnAl–CrO_4 were calcined for 3 h in static air at 250, 400, 600 and 800 °C, while samples CdAlCr-N-X and CdAl–CrO_4 were calcined at 150, 300, 500 and 800 °C. The PXRD patterns for all original samples and the calcined products are included in Figs. 6 and 7.

Calcination at 250 °C of sample ZnAlCr-C-∞ produces the collapse of the layered structure, although it is still possible to detect a poorly defined peak due to diffraction by planes (1 1 0) of the hydrotalcite phase, and weak diffraction lines corresponding to ZnO are identified; this means that this phase crystallizes even at the first stages of destruction of the layered structure [50]. The behavior observed for the Cr-containing samples is, however, different; so, sample ZnAlCr-C-1 shows extremely weak signals (compare the scale used to plot its diagram with those for the other samples), where some weak maxima due to the hydrotalcite phase are still detected. This effect is even much more evident for sample ZnAlCr-C-0, which PXRD diagram after calcination at 250 °C is almost coincident with that for the original. In other words, the presence of Cr^{3+} ions increases the stability of the hydrotalcite structure.

This effect is also observed when the calcination temperature is increased to 400 °C. The diagram for simple ZnAlCr-C-∞ is very similar to that recorded for the simple calcined at 250 °C, but the maximum due to planes (1 1 0) of the hydrotalcite phase has vanished and those due to ZnO are reinforced, new maxima due to this phase also developing at larger 2 theta values. The hydrotalcite-phase maxima have completely disappeared in the diagram of sample ZnAlCr-C-1 calcined at 400 °C, and new maxima, due to ZnO,

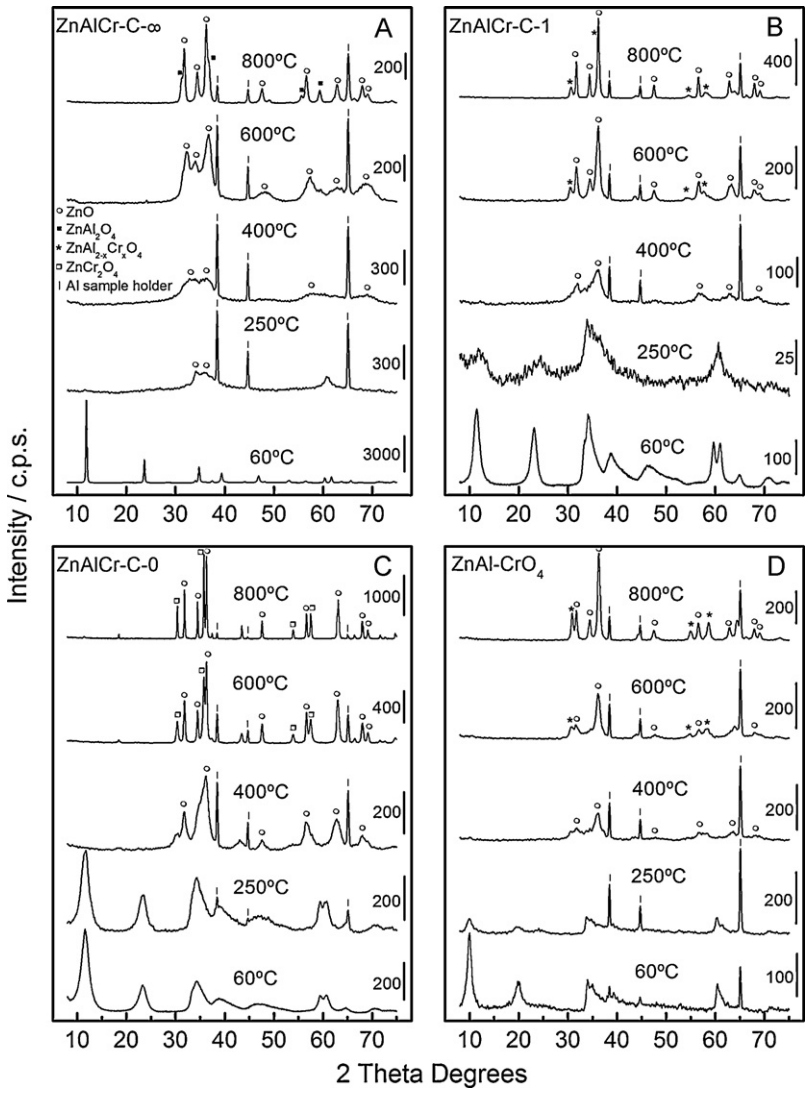

Fig. 6. PXRD diagrams of the calcined samples ZnAlCr-C and calcined sample ZnAl–CrO_4 at different temperatures.

better crystallized than in sample ZnAlCr-C-∞–400, are recorded. The maxima are even more intense and are better defined for sample ZnAlCr-C-0 calcined at this same temperature. However, the asymmetry of some of the diffraction maxima suggests the probable presence of other phases. In other words: while the presence of chromium in the brucite-like layers seems to stabilize this phase at low calcination temperature, when this is increased decomposition and crystallization of ZnO seems to be favoured.

Further increasing of the calcination temperature to 600 and 800 °C has a similar effect on all three samples, namely, a sharpening of the maxima due to the ZnO phase and a clear identification of maxima due to other phases, which nature depends on the chemical composition of the original sample. So, sample ZnAlCr-C-0 calcined at 600 °C shows maxima due to ZnO and $ZnCr_2O_4$, while the simultaneous presence of Al and Cr in sample ZnACr-C-1 gives rise, in addition to formation of ZnO, to a new phase which diffraction maxima are recorded just between those corresponding to $ZnAl_2O_4$ and $ZnCr_2O_4$; we have tentatively formulated this phase as $ZnAl_{2-x}Cr_xO_4$. This result is not unexpected, because the similarities of the ionic radii of Al^{3+} and Cr^{3+}. Only maxima due to ZnO are still recorded for sample ZnAlCr-C-∞. After calcination at 800 °C the maxima due to ZnO (in all three cases), $ZnAl_{2-x}Cr_xO_4$ (in sample ZnAlCr-C-1) and $ZnAl_2O_4$ or $ZnCr_2O_4$ (for samples ZnAlCr-C-∞ and ZnAlCr-C-0, respectively) are rather sharp, the most intense ones being those due to ZnO, in agreement with the largest molar fraction of Zn with respect of the other cations. It should be stressed that in the original samples the Zn/trivalent cation molar ratio is very close to 2 (see Table 4), while in the spinels such a ratio is 0.5, and consequently segregation of ZnO, in addition to a spinel phase, is expected [8].

The thermal decomposition can be outlined as follows, although we indicate in these reactions only the crystal phases that have been clearly identified:

$$\text{ZnAlCr-C-}\infty \xrightarrow{250\,^\circ\text{C}} \text{ZnO} + \text{ZnAlCr-C-}\infty \xrightarrow{400-600\,^\circ\text{C}} \text{ZnO} \xrightarrow{800\,^\circ\text{C}} \text{ZnO} + ZnAl_2O_4$$

$$\text{ZnAlCr-C-1} \xrightarrow{250\,^\circ\text{C}} \text{ZnO} + \text{ZnAlCr-C-1} \xrightarrow{400\,^\circ\text{C}} \text{ZnO} \xrightarrow{600-800\,^\circ\text{C}} \text{ZnO} + ZnAl_{2-x}Cr_xO_4$$

$$\text{ZnAlCr-C-0} \xrightarrow{250\,^\circ\text{C}} \text{ZnAlCr-C-0} \xrightarrow{400-800\,^\circ\text{C}} \text{ZnO} + ZnCr_2O_4$$

Regarding the thermal decomposition of the sample with chromate in the interlayer (Fig. 6D), a residual layered structure remains after calcination at 250 °C, although the maxima are very weak. Collapsing of the structure is observed after heating at 400 °C, and broad diffraction maxima are recorded, suggesting the presence of

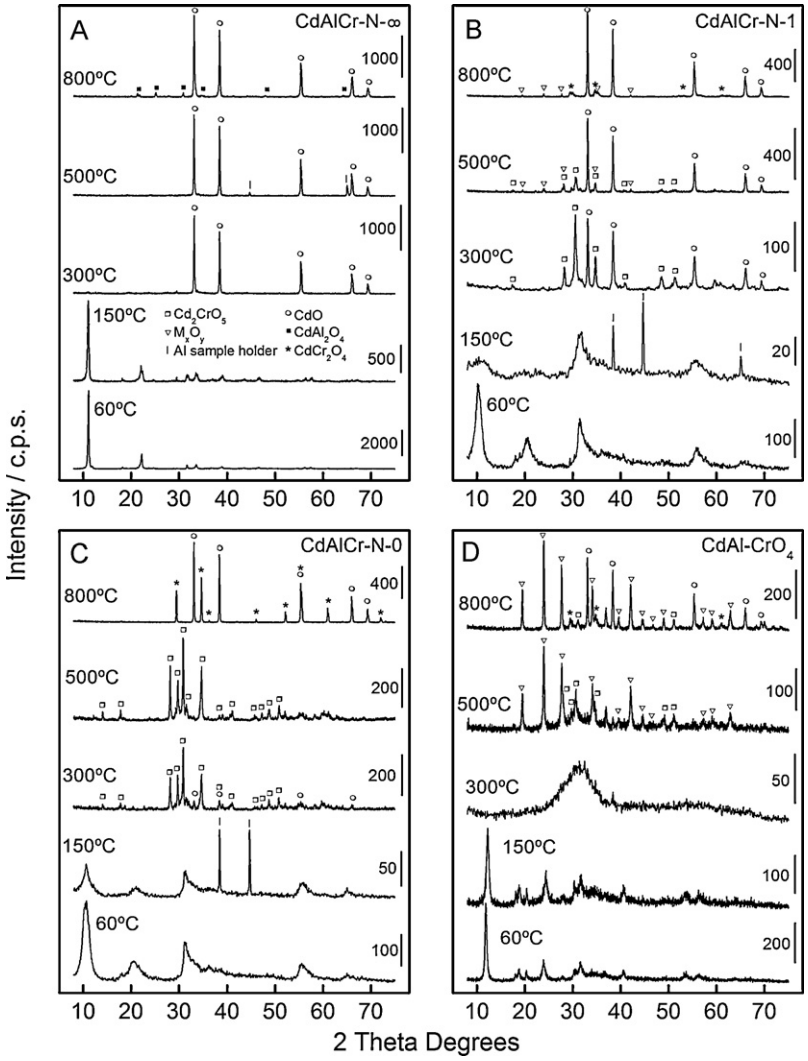

Fig. 7. PXRD diagrams of the calcined samples CdAlCr-N and calcined sample CdAl–CrO_4 at different temperatures.

mostly amorphous phases, probably related to ZnO and a spinel phase. The crystallinity of the both phases, ZnO and the spinel, increases at 600–800 °C, giving rise to narrower and more intense lines in the diagram. The maxima corresponding to the spinel phase appear again in an intermediate position between those corresponding to $ZnAl_2O_4$ and $ZnCr_2O_4$, according to the formation of a $ZnAl_{2-x}Cr_xO_4$ solid solution also in this case. A schematic representation of the changes in the structure is shown in graphical abstract. The thermal decomposition can be represented by the following equation:

$$ZnAl\text{–}CrO_4 \overset{250\,^{\circ}C}{\longrightarrow} ZnO + ZnAl\text{–}CrO_4 \overset{400\text{–}800\,^{\circ}C}{\longrightarrow} ZnO + ZnAl_{2-x}Cr_xO_4$$

It is evident that the crystalline phases along the calcination process and at the maximum temperature reached depend on the chemical composition of the original solids. However, it is worthwhile to check the behavior shown by samples ZnAlCr-C-1 and ZnAl–CrO_4, with similar chromium contents. First of all, on calcining the samples at 250 °C remains of the layered structure seems to exist, although the signals are very weak. On calcination at 400 °C the hydrotalcite-phase is completely disappeared in the diagram. After calcination at 600 °C the maxima due to ZnO are more intense, if compared to those of the solid solution spinel, for sample ZnAlCr-C-1, and this difference is also observed for the samples calcined at 800 °C. It seems that location of the chromium species in the interlayer in some sort of way delays formation of the spinel phase, and even when it is formed, its molar fraction is lower than that for the other sample; we should not forget, also, that interlayer chromate ought to be reduced to the trivalent state before the spinel phase is formed, and this might also give rise to its delayed formation.

Fig. 7A–C shows the PXRD diagrams of samples CdAlCr-N-X and their calcination products at different temperatures. Samples calcinated at 150 °C still mostly retain the layered hydrotalcite structure, although the maxima are markedly weaker than for the original, uncalcined samples. After calcination at 300 °C, the layered structure has been completely destroyed and reflections corresponding to a Cd_2CrO_5 phase (JCPDS: 21-0826) [19] and to CdO (JCPDS: 05-0640) [19] are recorded for all samples containing Cr. Obviously, sample CdAlCr-N-∞ calcined at 300 °C shows only maxima due to CdO. The maxima corresponding to CdO are very weak for sample CdAlCr-N-0, probably because most of Cd should be forming Cd_2CrO_5 in agreement with the Cd/Cr ratio in the pristine hydrotalcite. However, the higher Cd/Cr ratio in sample CdAlCr-N-1 could explain the somewhat larger intensity of the CdO lines recorded for this sample. No maxima corresponding to aluminum-containing phases is recorded for any of the samples, but a slight shift in the position of the diffraction maxima is observed, if compared to those for the pure oxides, suggesting that the Al^{3+} species could be dissolved in the structure of the other oxides, as previously reported

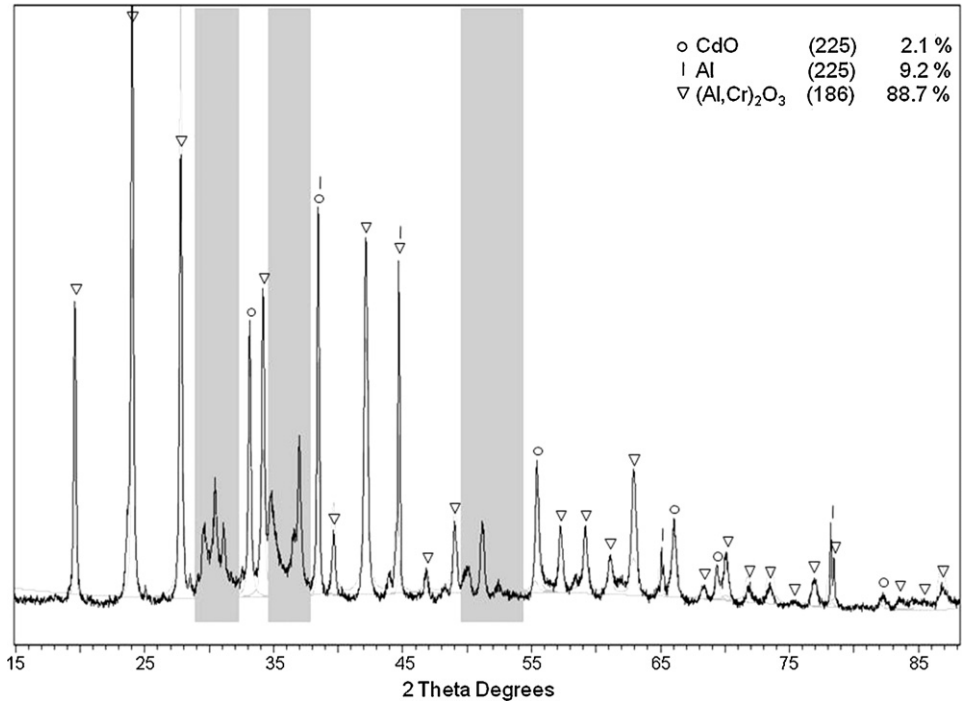

Fig. 8. Final adjustment obtained through the Powder Cell 2.4 of PXRD diagram of sample CdAl–CrO_4 calcined at 800 °C. The regions excluded in the fitting have been marked.

for Mg–Al or Ni–Al [51] or Cd–Al [8] hydrotalcites. It should be also noticed that the relative intensities of the diffraction lines has increased markedly for all three samples, but specially for sample CdAlCr-N-∞.

No signal due to Al^{3+} containing phases is recorded either in the diagram of sample CdAlCr-N-∞ calcined at 500 °C, which diagram is almost coincident to that for the sample calcined at 300 °C. Similarly, the maxima recorded for sample CdAlCr-N-0 calcined at 500 °C are the same, but more intense, as for the sample calcined at 300 °C. However, new maxima develop for sample CdAlCr-N-1 calcined at 500 °C. As for the set of Zn-containing samples studied above, it seems that the simultaneous presence of Cr and Al cations in the layers determines the nature of the phases formed. In this case, the new maxima, in addition to those due to CdO and Cd_2CrO_5, cannot be ascribed to any of the crystalline phases existing in the JCPDS database. We will name this new phase as M_xO_y and we will turn below to its possible nature.

Finally, after calcination at 800 °C, a single spinel phase ($CdAl_2O_4$ or $CdCr_2O_4$) has been identified for samples with only a trivalent metal cation in the layer, together with a well crystallized CdO phase in both cases (Fig. 7A and C). Regarding sample CdAlCr-N-1, intense maxima due to CdO, very weak ones due to the $CdCr_2O_4$ spinel (JCPDS: 17-0319) [19] and weak (as for the sample calcined at 500 °C) ones due to the M_xO_y oxide can be observed. The increase of the calcination temperature from 500 to 800 °C leads to formation of $CdCr_2O_4$ as a result of the reduction from Cr^{6+} to Cr^{3+}, as it has been concluded from the DTA/TG results and analysis of the evolved gases. On the other hand, the position of the diffraction lines of the spinel phase appear slightly shifted towards smaller spacing values. This can be attributed to the incorporation of Al^{3+} cation in the structure of the spinel $CdCr_2O_4$ (see scheme decomposition). However, the positions of these maxima match with the pattern of the $CdCr_2O_4$ spinel (JCPDS: 17-0319) [19] for the Al-free sample CdAlCr-N-0.

Based on these results, the thermal decomposition process of these samples can be outlined as follows:

$$\text{CdAlCr-N-}\infty \xrightarrow{300-500\,^{\circ}\text{C}} \text{Cd(Al))O} \xrightarrow{800\,^{\circ}\text{C}} \text{Cd(Al)O} + CdAl_2O_4$$

$$\text{CdAlCr-N-1} \xrightarrow{300\,^{\circ}\text{C}} \text{Cd(Al)O} + Cd_2CrO_5 \xrightarrow{500\,^{\circ}\text{C}} \text{Cd(Al)O} + Cd_2CrO_5 + M_xO_y \xrightarrow{800\,^{\circ}\text{C}} \text{CdO} + CdCr_{2-x}Al_xO_4 + M_xO_y$$

$$\text{CdAlCr-N-0} \xrightarrow{300\,^{\circ}\text{C}} \text{CdO} + Cd_2CrO_5 \xrightarrow{500\,^{\circ}\text{C}} Cd_2CrO_5 \xrightarrow{800\,^{\circ}\text{C}} \text{CdO} + CdCr_2O_4$$

The presence of Cr^{3+} in the layer leads to the formation of the mixed oxide, Cd_2CrO_5, involving oxidation of Cr^{3+} to Cr^{6+}, at 300–500 °C, depending on the precise composition of the solid. However, calcination at 800 °C leads to formation of the $CdCr_2O_4$ spinel that involves the reduction of Cr^{6+} to Cr^{3+}.

Regarding the thermal decomposition of the sample with interlayer chromate (Fig. 7D), it has been observed that, after calcination at 150 °C, the layered structure is roughly maintained, although the diffraction maximum corresponding to planes (0 0 3) shifts to higher angles, indicating a decrease in the interlayer spacing. This fact should be related to the *grafting* process [26,52,53] above mentioned, leading to a narrowing of layer. After heating at 300 °C total collapsing of the layer structure takes place, and only a broad diffraction entered about 30° (2θ) is recorded. The X-ray diffraction diagram shows only a broad line and it is not possible to determine the presence of any crystalline phase. Location of chromium species in the interlayer instead of in the layer hinders (or, at least, delays) the formation of crystalline oxides and higher temperatures are required to trigger diffusion of metal cations. This behavior is similar to that previously observed for the Cd(Al + Fe) system [8]. Calcination at 500 °C produces an increase in the crystallinity of the phases enabling the identification of the diffraction lines of Cd_2CrO_5 and M_xO_y. Quite surprisingly, CdO, which was formed at 300 °C for the other samples here studied, was not detected. Finally, four phases can be identified, namely, CdO, $CdCr_2O_4$, Cd_2CrO_5 and M_xO_y upon heating at 800 °C.

The more intense diffraction lines for this unknown phase M_xO_y are recorded at 4.53, 3.70, 3.21 and 2.14 Å, and it becomes the dominant phase when chromium is in the interlayer as chromate (CdAl–CrO_4 calcined at 800 °C), segregating CdO which has not been detected when the sample had been calcined at 500 °C. For this reason, this sample calcined at 800 °C has been used for the

Table 6
Rietveld refinement results (standard deviation in parenthesis).

	Al holder	CdO	$(Al,Cr)_2O_3$
Space group	*Fm*3*m* (225)	*Fm*3*m* (225)	*P*63*mc* (186)
Lattice parameters			
a	4.0649(2) Å	4.6976(3) Å	5.2639(2) Å
c			12.8947(4) Å
Weight percentage (%)	2.09(1)	9.18(2)	88.73(5)
Statistical indices	R_p = 29.88; R_{wp} = 36.82; R_{exp} = 0.26		

identification of the M_xO_y phase, from a slowly recorded ($0.15^\circ 2\theta\,min^{-1}$) X-ray diffraction profile and fitting the data by using the Powder Cell 2.4 program [54]. The Powder Cell provides a very easy interface to perform simple Le Bail fitting.

Fitting of the diagram was made from the following data: a cubic cell for the Al sample holder, space group *Fm*3*m* (No. 225) with unit cell parameter *a* = 4.0469 Å (JCPDS: 04-0787) [19]; a cubic cell and the same space group for the CdO, with *a* = 4.6953 Å (JCPDS: 05-0640) [19]; a hexagonal cell with a space group *P*63*mc* (no. 186) (JCPDS: 26-0031) [19] for the phase M_xO_y, for which we will assume a composition $(Al,Cr)_2O_3$, where Al and Cr atoms are randomly located at crystallographic positions 6c, and O atoms in 12d positions. The starting cell parameters were *a* = 5.25 Å and *c* = 12.90 Å, and the position coordinates were (0.5000, 0.5000, 1.0000) for 6c and (0.3059, 0.0000, 0.2500) for 12d.

The best fit reached is included in Fig. 8; the grey zones in this graph have been excluded from the fitting with the goal to improve it, because in these areas diffraction lines due to other minor phases, such as $CdCr_2O_4$ and Cd_2CrO_5, are recorded. The final adjustment shows that the major phase is the $(Al,Cr)_2O_3$ oxide (88.7%) with *a* = 5.2639 Å and *c* = 12.8947 Å, CdO amounting only 2.1% and the Al sample holder lines 9.2%. The quality of the adjustment is defined by the values R_p = 29.88, R_{wp} = 36.82 and R_{exp} = 0.26 (Table 6).

The calcination process of the hydrotalcite sample with interlayer chromate can be outlined as follows:

$$CdAl\text{–}CrO_4 \overset{500^\circ C}{\longrightarrow} Cd_2CrO_5 + (Al,Cr)_2O_3 \overset{800^\circ C}{\longrightarrow} CdO + (Al,Cr)_2O_3 + CdCr_2O_4 + Cd_2CrO_5$$

It can be concluded that the decomposition process of samples CdAlCr-N-X gives rise to the formation of Cd_2CrO_5 between 300 and 500 °C due to oxidation of Cr^{3+} to Cr^{6+} and formation of CdO and $CdCr_2O_4$ spinel at higher temperatures (800 °C), and only when the sample contains both trivalent metals a $(Al,Cr)_2O_3$ mixed oxide is also formed. When chromium is in the interlayer space, the dominant phase (between 500 and 800 °C) is $(Al,Cr)_2O_3$ instead of CdO, as occurs for hydrotalcite CdAlCr-N-1. This result is in agreement with the lower Cd content in the $CdAl\text{–}CrO_4$ hydrotalcite (Table 4).

4. Conclusions

Layered double hydroxides with the hydrotalcite-like structure, containing Cd/Zn and Al, and with Cr located in the layer, or in the interlayer as chromate, have been prepared.

The presence of Cr^{3+} in the layer of samples MAlCr-I-X gives rise to an increase in their thermal stability. Likewise, the intercalation of the chromate oxoanion also produces an increase in the thermal stability of the compound due to a "grafting" process.

Hydrotalcites with Zn as divalent cation and only a trivalent one (Al,Cr) in the layer decompose forming ZnO and the corresponding spinel, $ZnAl_2O_4$ or $ZnCr_2O_4$. However, samples containing Al in the layer and chromium in the layer or in the interlayer give rise, in all cases, to the formation of a $ZnAl_{2-x}Cr_xO_4$ solid solution with the spinel structure. Chromate species in sample $ZnAl\text{–}CrO_4$ undergo a reduction process when the solid is heated at 800 °C.

Calcination of hydrotalcite CdAlCr-N-1 at moderate temperatures produces an oxidation of chromium from Cr^{3+} to Cr^{6+} to form a Cd_2CrO_5 mixed oxide, Cr^{6+} species being reduced again reduced at higher temperatures. Consequently, the presence of a well crystallized phase with the spinel structure $CdCr_2O_4$, CdO and the mixed oxide $(Al,Cr)_2O_3$ are detected at 800 °C.

Calcination of the $CdAl\text{–}CrO_4$ hydrotalcite at 500 °C gives rise to the formation of $(Al,Cr)_2O_3$ and Cd_2CrO_5. At higher calcination temperatures (800 °C) $(Al,Cr)_2O_3$ was detected as the major phase, together with CdO, Cd_2CrO_5 and $CdCr_2O_4$ as minor ones.

We can conclude that the evolution of calcination products is determined by the nature of the divalent metal, Cd or Zn, in the structure of the hydrotalcite.

Acknowledgements

This work has been partially supported by grant MAT2009-08526 from MICINN and Junta de Andalucía through Research Group FQM-214; funding from ERDF is also acknowledged.

References

[1] F. Bergaya, G. Lagaly, General introduction: clays clay mineral and clay science. P10, in: F. Bergaya, B.K.G. Theng, G. Lagaly (Eds.), Handbook of Clay Science: Developments in Clay Science, vol. 1, Elsevier, Amsterdan, 2006.
[2] J. He, M. Wei, B. Li, Y.D. Kang, G. Evans, X. Duan, Struct. Bond. 119 (2006) 89–119.
[3] J.S. Valente, J. Hernández-Cortez, M.S. Cantu, G. Ferrat, E. López-Salinas, Catal. Today 150 (2010) 340–345.
[4] P. Benito, F.M. Labajos, V. Rives, J. Solid State Chem. 179 (2006) 3784–3797.
[5] W. Meng, F. Li, D.G. Evans, X. Duan, J. Mater. Sci. 39 (2004) 4655–4657.
[6] D.G. Evans, X. Duan, Chem. Commun. 5 (2006) 485–496.
[7] Y. Guo, H. Zhang, L. Zhao, G.-D. Li, J.-S. Chen, L. Xu, J. Solid State Chem. 178 (2005) 1830–1836.
[8] M.R. Pérez, C. Barriga, J.M. Fernández, V. Rives, M.A. Ulibarri, J. Solid State Chem. 180 (2007) 3434–3442.
[9] J.M. Fernández, C. Barriga, M.A. Ulibarri, F.M. Labajos, V. Rives, Chem. Mater. 9 (1997) 312–318.
[10] A. Mantilla, F. Tzompantzi, J.L. Fernández, J.A.I. Díaz Góngora, G. Mendoza, R. Gómez, Catal. Today 148 (2010) 119–123.
[11] C. Karunakaran, S. Senthilvelan, Curr. Sci. India 88 (2005) 962–967.
[12] C. Karunakaran, R. Dhanalakshmi, Sol. Energy Mater. Sol. Cells 92 (2008) 1315–1321.
[13] Karunakaran, R. Dhanalakshmi, P. Gomathisankar, G. Manikandan, J. Hazard. Mater. 176 (2010) 799–806.
[14] F. Kooli, K. Kosuge, A. Tsunashima, J. Solid State Chem. 118 (1995) 285–291.
[15] F. Kooli, V. Rives, M.A. Ulibarri, W. Jones, Mater. Res. Soc. Symp. 371 (1995) 143–149.
[16] I. Crespo, C. Barriga, M.A. Ulibarri, G. González-Bandera, P. Malet, V. Rives, Chem. Mater. 13 (2001) 1518–1527.
[17] F. Li, X. Duan, Struct. Bond. 119 (2006) 193–223.
[18] V. Rives, D. Carriazo, C. Martín, Heterogeneous catalysis by polyoxometalate-intercalated layered double hydroxides, in: A. Gil, S.A. Korili, R. Trujillano, M.A. Vicente (Eds.), Pillared Clays and Related Catalysts, Springer, 2010 (Chapter 12).
[19] Joint Committee on Powder Diffraction Standard-International Centre for Diffraction Data, Swarthmore, PA, 1995.
[20] A.S. Bookin, V.A. Drits, Clays Clay Miner. 41 (1993) 551–557.
[21] J. Rodríguez-Carvajal, Program of Structure Fitting, AFFMA, Version PC, 1987.
[22] G.W. Brindley, S. Kikkawa, Am. Mineral. 64 (1979) 836–843.
[23] G. Brown, in: G.W. Brindley, G. Brown (Eds.), Crystal Structures of Clay Minerals and their X-ray Identification, Mineralogical Society, London, 1980, p. 397.
[24] J.E. Huheey, E.A. Keiter, R.L. Keiter, Inorganic Chemistry: Principles of Structure and Reactivity, 4th ed., Harper Collins College Publishers, New York, 1993.
[25] S. Miyata, T. Kumura, H. Hattori, K. Tanabe, Nippon Kagaku Zasshi 92 (1971) 514–517.
[26] F. Malherbe, L. Bigey, C. Forano, A. de Roy, J.P. Besse, J. Chem. Soc., Dalton Trans. 21 (1999) 3831–3839.
[27] V.A. Drits, R.S. Bookin, in: V. Rives (Ed.), Layered Double Hydroxides: Presents and Future, Nova Science Publishers, New York, 2001, p. 39.
[28] D.G. Evans, R.C.T. Slade, Struct. Bond. 119 (2006) 1–87.
[29] T. Kwon, G.A. Tsigdinos, T.J. Pinnavaia, J. Am. Chem. Soc. 110 (1988) 3653–3654.
[30] S. Miyata, A. Okada, Clays Clay Miner. 25 (1977) 14–18.
[31] M. del Arco, D. Carriazo, C. Martin, A.M. Pérez-Grueso, V. Rives, J. Solid State Chem. 178 (2005) 3571–3580.
[32] V. Rives, M.A. Ulibarri, Coord. Chem. Rev. 181 (1999) 61–120.
[33] A. de Roy, C. Forano, J.P. Besse, in: V. Rives (Ed.), Layered Double Hydroxides: Present and Future, Nova Science Publishers, New York, 2001, p. 1.
[34] F.M. Labajos, V. Rives, M.A. Ulibarrri, J. Mater. Sci. 27 (1992) 1546–1552.

[35] E.L. Crepaldi, P.C. Pavan, J. Tronto, J.B. Valim, J. Colloid Interface Sci. 248 (2002) 429–442.
[36] J.T. Kloprogge, L. Hickey, R.L. Frost, Mater. Chem. Phys. 89 (2005) 99–109.
[37] J.T. Kloprogge, R.L. Frost, in: V. Rives (Ed.), Layered Double Hydroxides: Present and Future, Nova Science Publishers, New York, 2001, p. 139.
[38] T. Hibino, Y. Yamashita, K. Kowge, A. Tsunashima, Clays Clay Miner. 43 (1995) 427–432.
[39] F.M. Labajos, V. Rives, M.A. Ulibarri, Spectrosc. Lett. 24 (1991) 499–508.
[40] M.J. Hernández-Moreno, M.A. Ulibarri, J.L. Rendón, C.J. Serna, Phys. Chem. Miner. 12 (1985) 34–38.
[41] K. Nakamoto, Infrared and Raman Spectra of Inorganic and Coordination Compounds, J. Wiley and Sons, New York, 2008.
[42] J.T. Kloprogge, Infrared and Raman spectroscopy of naturally occurring hydrotalcites and their synthetic equivalent, in: J.T. Kloprogge (Ed.), The Application of Vibrational Spectroscopy to Clay Minerals and Layered Double Hydroxides, CMS Workshop Lectures, vol. 13, The Clay Mineral Society, Aurora, CO, 2005, p. 203.
[43] S. Miyata, Clays Clay Miner. 23 (1975) 369–370.
[44] F.M. Labajos, V. Rives, Inorg. Chem. 35 (1996) 5313–5318.
[45] V. Rives, in: V. Rives (Ed.), Layered Double Hydroxides: Present and Future, Nova Science Publishers, New York, 2001, p. 115.
[46] R.C. West (Ed.), Handbook of Chemistry and Physics, 91st ed., CRC Press, Inc., Cleveland, Ohio, 2010.
[47] F. Cavani, F. Trifirò, A. Vaccari, Catal. Today 11 (1991) 173–301.
[48] M.J. Hudson, S. Carlino, D.C. Apperley, J. Mater. Chem. 5 (1995) 323–329.
[49] Ts. Stanimirova, N. Piperov, N. Petrova, G. Kirov, Clay Miner. 39 (2004) 177–191.
[50] K. El Malki, A. de Roy, J.P. Besse, Mater. Res. Bull. 28 (1993) 667–673.
[51] T. Sato, K. Kato, T. Endo, M. Shimada, React. Solids 2 (1986) 253–260.
[52] F. Malherbe, J.P. Besse, J. Solid State Chem. 155 (2000) 332–341.
[53] C. Depège, C. Forano, A. de Roy, J.P. Besse, Mol. Cryst. Liq. Cryst. 244 (1994) 161–166.
[54] W. Kraus, G. Nolze, J. Appl. Crystallogr. 29 (1996) 301–303.